Available online at www.sciencedirect.com
SCIENCE DIRECT®
International Journal of Heat and Mass Transfer 47 (2004) 4215–4231
International Journal of HEAT and MASS TRANSFER
www.elsevier.com/locate/ijhmt

Three-dimensional analysis of heat transfer in a micro-heat sink with single phase flow

J. Li [a], G.P. Peterson [a,*], P. Cheng [b]

[a] Department of Mechanical, Aerospace and Nuclear Engineering, Rensselaer Polytechnic Institute, 110 8th Street, Troy, NY 12180, USA

[b] School of Mechanical and Power Engineering, Shanghai Jiaotong University, Shanghai 200030, PR China

Received 29 March 2004; received in revised form 30 April 2004

Abstract

A detailed numerical simulation of forced convection heat transfer occurring in silicon-based microchannel heat sinks has been conducted using a simplified three-dimensional conjugate heat transfer model (2D fluid flow and 3D heat transfer). The micro-heat sink model consists of a 10 mm long silicon substrate, with rectangular microchannels, 57 μm wide and 180 μm deep, fabricated along the entire length. A finite difference numerical code with a Tri-Diagonal Matrix Algorithm (TDMA) was developed to solve the governing equations. The validated code provided detailed temperature and heat flux distributions in the microchannel heat sink. The influence of the geometric parameters of the channel and the thermophysical properties of the fluid on the flow and heat transfer, are investigated by evaluating thermophysical properties at a reference bulk temperature. The results indicate that thermophysical properties of the liquid can significantly influence both the flow and heat transfer in the microchannel heat sink. The bulk liquid temperature is shown to vary in a quasi-linear form along the flow direction for high fluid flow rates, but not for low flow rates. Comparison of the numerical results with other published numerical results and experimental data available in the literature for Reynolds numbers less than 200 based on a hydraulic diameter of $D_h = 86$ μm and $D_h/L_x < 0.01$, indicates that the assumption of hydrodynamic, fully developed laminar flow is valid. The thermal entrance length is also obtained from the detailed local heat transfer coefficient calculation and a correlation for the overall averaged Nusselt number is developed and discussed. Finally, a methodology is proposed whereby measured data can be evaluated and processed in order to provide a more complete understanding and better interpretation of these experimental data.

Keywords: Microchannel; Numerical simulation; Heat transfer; Electronic cooling

1. Introduction

Recent advances in very large-scale integration (VLSI) technology and Micro-Electro Mechanical Systems (MEMS), have resulted in the ability to fabricate many heretofore unimagined mechanical and/or electromechanical devices on a single silicon wafer. Because microchannels with noncircular cross-sections comprise an integral part of these silicon-based microsystems and may be heated asymmetrically, functional designs require that the fluid flow and heat transfer characteristics in these microchannels be known and understood. In addition, the microminiaturization of electronic devices and resulting increased packaging density and associated high heat fluxes [1], require novel cooling strategies that may involve the silicon-based microchannel heat sinks.

For more than a decade, investigations have been conducted to better understand the fluid flow and heat transfer characteristics in silicon-based microchannel

* Corresponding author. Tel.: +1-518-276-6487; fax: +1-518-276-4061.
E-mail address: peterson@rpi.edu (G.P. Peterson).

0017-9310/$ - see front matter © 2004 Elsevier Ltd. All rights reserved.
doi:10.1016/j.ijheatmasstransfer.2004.04.018

Nomenclature

A	area of cross-section of microchannel
A_w	area of substrate bottom wall
C_P	specific heat
f	friction factor
H	height of channel
h	convective heat transfer coefficient
L	length of microchannel
L_m	length of side wall of cavity
$\dot{m}$	mass flow rate
N	total number of grids in mesh
Nu	Nusselt number
$\overline{Nu}_{definition}$	averaged Nusselt number from definition of Eq. (28)
$\overline{Nu}_{eq}$	overall equivalent Nusselt number in Eq. (25)
$\overline{Nu}_{rough}$	roughly averaged Nusselt number from Eqs. (26) and (27)
P	pressure
q_w	heat flux
Re	Reynolds number
S	total surface area of inner wall of channel
T	temperature
T_w	temperature at wall of microchannel
u	x-direction velocity of liquid
$\boldsymbol{V}$	vector of velocity
W	width of channel

Greek symbols

λ	conductivity
ρ	density
μ	dynamic viscosity
υ	kinetic viscosity
Γ	periphery of the inner wall of channel

Subscripts

ave	averaged value
con	conservation of energy
e	entrance effects
h	hydrodynamic equivalent value
in	at inlet of channel
l	liquid
m	mean value
num	numerical results
out	at outlet of channel
s	surface of channel; Solid
w	substrate wall
x	local value along the longitudinal direction

heat sinks designed for applications in electronic cooling. These noncircular channels and silicon based microchannel heat sinks combine the attributes of high material compatibility, high surface area per unit volume ratios, and large potential heat transfer performance, with highly sophisticated and economic fabrication processes. These advantages make these silicon based microchannel heat sinks extremely attractive for a wide variety of commercial applications. Comparison of the experimental results, however, indicates a number of disparities between the values predicted using classical macromodeling techniques and the experimental data available in the literature. In addition, there appears to be considerable variation in the experimental data obtained by various investigators [2,3].

It is well known that the cross-sectional shape of a channel can have significant influence on the fluid flow and heat transfer characteristics in noncircular microchannels. Peng and Peterson [4] performed experimental investigations of the pressure drop and convective heat transfer for water flowing in rectangular microchannels, and found that the cross-sectional aspect ratio had significant influence on the flow friction and convective heat transfer in both laminar and turbulent flows. Kawano et al. [5] provided experimental data on the friction and heat transfer in rectangular, silicon based microchannel heat sinks, and more recently Wu and Cheng [6,7] conducted a series of experiments to measure the friction factor and convective heat transfer in smooth silicon microchannels of trapezoidal cross-section. However, the experimental test articles [2–7] for the various experimental investigations vary greatly, making it very difficult to compare the experimental results or to draw any significant, experimentally substantiated conclusions. In addition, the derived empirical correlations may differ from each other, with each only applicable for the geometry of that particular heat sink and fabrication process. This is especially true when comparing results from single channels with that obtained in multichannel flow. For these reasons, it is necessary not only to conduct experimental investigations, but also to develop numerical models that are capable of providing insight to the fundamental physics that govern the fluid flow and heat transfer characteristics of these microchannel heat sinks.

It is important to note that in silicon-based MEMS technology, unlike larger-scale conventional heat exchangers, microchannels fabricated as an integral part of silicon wafers, often have noncircular cross-sections due to the fabrication processes used, i.e., trapezoidal, triangular or rectangular. In addition, the heat source is usually located on only one side of the channel, as opposed to the case where the perimeter of the channel is heated symmetrically. In the earliest analytical studies of

heat transfer in microchannel heat sinks, classical fin analysis methods were widely utilized and the results directly applied to model the heat transfer [8,9]. While this presents a reasonable first approximation, there exist a number of assumptions in this classical method, which when combined, significantly reduces the accuracy of the results as noted by Qu and Mudawar [10].

Wesberg et al. [11] solved a two-dimensional conjugate heat transfer problem for microchannel heat sinks to obtain detailed spatial distributions of the temperature of the heat sink cross-section along the length of the channels. Fedorov and Viskanta [12] developed a three-dimensional model to investigate the conjugate heat transfer in a microchannel heat sink with the same channel geometry used in the experimental work done by Kawano et al. [5]. This investigation indicated that the average channel wall temperature along the flow direction was nearly uniform except in the region close to the channel inlet, where very large temperature gradients were observed. Qu and Mudawar [10] conducted a three-dimensional fluid flow and heat transfer analysis for a rectangular microchannel heat sink with a geometry similar to that of Kawano et al. [5] using a numerical method similar to that proposed by both Kawano et al. [5] and Fedorov and Viskanta [12]. This model considered the hydrodynamic and thermal developing flow along the channel and found that the Reynolds number will influence the length of the developing flow region. It was also found that the highest temperature is typically encountered at the heated base surface of the heat sink immediately adjacent to the channel outlet, and that the temperature rise along the flow direction in the solid and fluid regions can both be approximated as linear.

While the general trends indicated above are similar, the numerical results achieved by Qu and Mudawar [10] and Fedorov and Viskanta [12] differ, and it is therefore necessary to clarify several important issues. The first of these is that while Qu and Mudawar [10] assumed constant fluid thermophysical properties, it is well known that the Reynolds number depends on the viscosity of the fluid, which changes significantly with the liquid bulk temperature. Fedorav and Viskanta [12] noted that the thermophysical properties are temperature dependent, but that modification of the thermophysical properties in the numerical calculation process were very difficult since the temperature and velocity of the liquid were coupled during the numerical calculation process. This coupling required that the thermal properties of the liquid, form one convergent solution with temperature at which time the velocity and temperature had to be recalculated. This process was then repeated until the final results had been achieved. In the method developed herein, the velocity field is first solved and then the mean velocity derived. The thermophysical properties are chosen at a reference temperature (an estimated averaged liquid bulk temperature) determined from the energy balance and then a new final velocity field and temperature distribution for the microchannel is defined.

The second issue of importance is that although the previous work provided some guidance and information about the behavior of the fluid flow field and heat transfer [10,12], some important *absolute values* were not presented, e.g., the total pressure drop along the flow direction and the velocity field. Finally, in order to accurately interpret the experimental data and to compare the measured data with the calculated results, it is necessary to properly define the overall Nusselt number at different Reynolds numbers.

In the current investigation, all three of these issues are addressed. A numerical model with fully developed flow is presented and used to analyze the heat transfer in a microchannel heat sink for low *Re* numbers (less than 150 on the basis of hydraulic diameter 86.58 μm). The numerical model is based upon a simplified three-dimensional conjugate heat transfer approach (2D fluid flow and 3D heat transfer). A series of calculations were carried out to analyze the transport process in a rectangular silicon-based microchannel heat sink with a geometry identical to that studied by Kawano et al. [5], Fedorov and Viskanta [12], and Qu and Mudawar [10]. Computations were performed for different total pressure drops in the channel to obtain the relation between the overall averaged *Nu* number and the *Re* number for this specific geometry of heat sinks.

2. Conjugate heat transfer in a micro-heat sink

The micro-heat sink modeled in this investigation consists of a 10 mm long silicon substrate with a silicon cover. The rectangular microchannels have a width of 57 μm and a depth of 180 μm. Using several different methods, the entrance length for the low Re number in the channel is identified. The averaged overall Nusselt number is carefully defined and after a series of calculations for different total pressure drops in the channel the relation between the overall Nusselt number and the Reynolds number is analyzed and discussed. These studies can help to clarify some of the variations in the previously published data and provide a fundamental insight into thermal and fluid transport process occurring in the microchannel heat sinks designed for electronic cooling and other applications.

Due to inconsistencies in the experimental results and an overall lack of understanding of the underlying nature of the phenomena, the classical Navier–Stokes and energy equations are used in the present study with no modifications made to account for the effects of surface characteristics on the fluid flow and heat transfer (such as roughness and hydrophilic properties or electric double layer).

A schematic of the rectangular microchannel heat sink is illustrated in Fig. 1 where a unit of cell consisting of one channel was selected because of the symmetry of the structure. The unit cell of the heat sink can be represented by an asymmetric rectangular channel with the cross-sectional dimensions as shown in Table 1. The channel geometry is identical to that employed in the experimental work of Kawano et al. [5] and in the numerical investigations of Qu and Mudawar [10] and Fedorov and Viskanta [12]. It is assumed that the power density input at the bottom of the heat sink is uniform.

The length required for the formation of a fully developed laminar profile in a microchannel can be estimated by the theoretical equation of Langhaar [13], developed for a round tube. Defining an entrance length, L_e as that distance required for the centerline velocity to reach 99% of the fully developed value. Langhaar's equation is,

$$\frac{L_e}{D_h} = 0.0575\frac{u_m D_h}{\upsilon} = 0.0575 Re_D \tag{1}$$

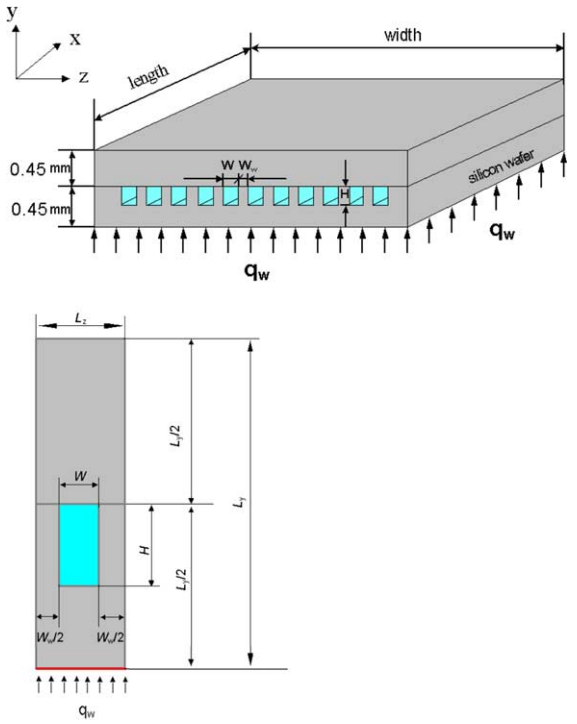

Fig. 1. Structure of a rectangle microchannel heat sink and the unit of cell.

Table 1
Geometric dimensions of the unit cell under consideration

H (μm)	W (μm)	W_w (μm)	D_h (μm)	L_y (μm)	L_z (μm)	L_x (mm)
180	57	43	86.58	900	100	10

The above holds true for Reynolds numbers of approximately 2000 or smaller based on the channel diameter. For a hydraulic diameter of $D_h = 86.58$ μm, this expression yields an entrance length of 634.3 μm for $Re = 140$. The pressure drop in the entrance region prior to the establishment of fully developed flow is much greater than for an equivalent length in the fully developed flow region, hence, the pressure drop calculated for fully developed flow will slightly underestimate the pressure drop in the actual situation. In Refs. [14–16], it is pointed out that the shape of the entrance is very important, with much shorter entrance lengths occurring for square-edged entrances than for rounded ones. Thus, because the flow entrance length may be less than 5% of the total length for a rectangular channel heat sink, the assumption of fully developed laminar flow over the entire length of the microchannel is acceptable for the heat transfer analysis, particularly in cases such as this where the Reynolds number is less than 150. This assumption is verified by the experimental results of Kawano et al. [5].

Consider a steady 3D flow in a silicon microchannel heat sink with heating from below and with adiabatic conditions at the other boundaries, as illustrated in Fig. 1, the symmetry of the heat sink yields a domain comprised of a unit cell with a single rectangular channel, shown schematically in Fig. 2. If the compressibility, the gravitational force and the dissipating heat caused by viscosity are neglected, the continuity, momentum and energy equations for a fully developed 3D flow heat transfer are,

$$\nabla \cdot \mathbf{v} = 0 \tag{2}$$

$$(\mathbf{v} \cdot \nabla)\mathbf{v} = -\frac{1}{\rho_l}\nabla P + \upsilon_l \nabla^2 \mathbf{v} \tag{3}$$

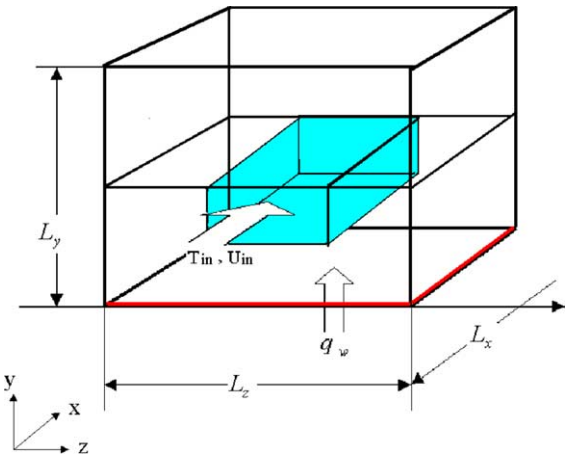

Fig. 2. Domain of numerical simulation.

$$\mathbf{v}\cdot\nabla T_{\mathrm{l}} = \frac{\lambda_{\mathrm{l}}}{C_P\rho_{\mathrm{l}}}\nabla^2 T_{\mathrm{l}} \tag{4}$$

respectively, and the hydrodynamic boundary conditions can be stated as:

$$u=0,\quad v=0,\quad w=0$$
at the inner wall surface (no-slip) (5a)

$$x=0,\quad P_{\mathrm{l}}=P_{\mathrm{in}},\quad v=0,\quad w=0$$
at the inlet, and (5b)

$$x=L_x,\quad P_{\mathrm{l}}=P_{\mathrm{out}}\quad(\text{here, 1atm}),\quad v=0,\quad w=0$$
at the outlet (5c)

For a steady, fully developed laminar flow, we have $\frac{\partial u}{\partial x}=0$ or $u=u(y,z)$, and $v=0$, $w=0$. Therefore, Eq. (3) with the boundary conditions given by Eq. (5) can be simplified to,

$$\frac{\partial^2 u}{\partial y^2}+\frac{\partial^2 u}{\partial z^2}=-\frac{1}{\mu_{\mathrm{l}}}\frac{\mathrm{d}P}{\mathrm{d}x}=-\frac{1}{\mu_{\mathrm{l}}}\frac{\Delta P}{L_x} \tag{6}$$

The energy equation for the liquid, Eq. (4), becomes

$$u\frac{\partial T_{\mathrm{l}}}{\partial x}=\frac{\lambda_{\mathrm{l}}}{C_P\rho_{\mathrm{l}}}\left(\frac{\partial^2 T_{\mathrm{l}}}{\partial x^2}+\frac{\partial^2 T_{\mathrm{l}}}{\partial y^2}+\frac{\partial^2 T_{\mathrm{l}}}{\partial z^2}\right) \tag{7}$$

The heat conduction in the silicon wafers is,

$$\frac{\partial}{\partial x}\left(\lambda\frac{\partial T_{\mathrm{w}}}{\partial x}\right)+\frac{\partial}{\partial y}\left(\lambda\frac{\partial T_{\mathrm{w}}}{\partial y}\right)+\frac{\partial}{\partial z}\left(\lambda\frac{\partial T_{\mathrm{w}}}{\partial z}\right)=0 \tag{8}$$

which is subject to the following thermal boundary conditions

$$y=0,\quad -\lambda_{\mathrm{w}}\frac{\partial T_{\mathrm{w}}}{\partial y}=q_{\mathrm{w}} \tag{9a}$$

$$y=L_y,\quad -\lambda_{\mathrm{w}}\frac{\partial T_{\mathrm{w}}}{\partial y}=0 \tag{9b}$$

$$x=0,\quad \text{if } (y,z)\in\text{channel } T_{\mathrm{l}}=T_{\mathrm{in}},$$
$$\text{else} -\lambda_{\mathrm{w}}\frac{\partial T_{\mathrm{w}}}{\partial x}=0 \tag{9c}$$

$$x=L_x,\quad \text{if } (y,z)\in\text{channel} -\lambda_{\mathrm{l}}\frac{\partial T_{\mathrm{l}}}{\partial x}=0,$$
$$\text{else} -\lambda_{\mathrm{w}}\frac{\partial T_{\mathrm{w}}}{\partial x}=0 \tag{9d}$$

$$z=0,\quad -\lambda_{\mathrm{w}}\frac{\partial T_{\mathrm{w}}}{\partial z}=0 \tag{9e}$$

$$z=L_z,\quad -\lambda_{\mathrm{w}}\frac{\partial T_{\mathrm{w}}}{\partial z}=0 \tag{9f}$$

$$-\lambda_{\mathrm{w}}\left(\left.\frac{\partial T_{\mathrm{w}}(x,y,z)}{\partial n}\right|_{\Gamma}\right)=-\lambda_{\mathrm{l}}\left(\left.\frac{\partial T_{\mathrm{l}}(x,y,z)}{\partial n}\right|_{\Gamma}\right),$$
at the inner wall surface (9g)

where, Eq. (9a) gives the uniform heat flux density boundary condition at the bottom wall of the wafer subjected to heating; Eqs. (9b)–(9f) assumes no heat loss from the solid to the ambient at the boundary except at $x=0$ for the liquid, where $T_{\mathrm{l}}=T_{\mathrm{in}}$; Eq. (9d) assumes a thermally fully developed flow at the outlet of the microchannel. It should be noted that in reality, heat losses from the heat sink to the environment should be considered by conduction and convection at the inlet and outlet and at the top surface of the heat sink. Eq. (9g) gives a matching heat flux boundary condition on the channel interface. Γ denotes the perimeter of the inner wall of the channel.

Eqs. (6)–(8) with the boundary conditions given in Eqs. (5) and (9) can be solved numerically. Initially, for the given pressure drops, ΔP, the 2D velocity profiles can be obtained from Eqs. (5) and (6). Once this has been done, the energy equations given by Eqs. (7)–(9) can be solved. The governing partial differential equations with the boundary conditions are then discretized by means of the control volume method with grid points placed at the center of each. The upwind scheme is used for the convection term in Eq. (7).

In this paper, a five-point difference scheme is used for Eq. (6) and a seven-point difference scheme is used for Eqs. (7) and (8). In order to expedite the convergence of the calculations, a line-by-line iteration and a Tri-Diagonal Matrix Algorithm (TDMA) method with a Thomas algorithm and successive under-relaxation iterative methods were used to obtain the 3D temperature distribution, $T(x,y,z)$. A more detailed explanation of the numerical solution can be found in Ref. [17].

The convergence criteria were established as

$$\sum\sum|u(j,k)-u_0(j,k)|\leqslant 10^{-3}\quad\text{for velocity, and} \tag{10}$$

$$\sum\sum\sum|T(i,j,k)-T_0(i,j,k)|\leqslant 10^{-2}\quad\text{for temperature} \tag{11}$$

The total grid number is 180,000 ($i(x)\times j(y)\times k(z)$ is $20\times90\times99$) for the domain. Eq. (11) yields an approximate criterion for the mean square root error (MSRE) of

$$|T(i,j,k)-T_0(i,j,k)|\approx\frac{\sum\sum\sum\sqrt{(T(i,j,k)-T_0(i,j,k))^2}}{N}\leqslant 5\times10^{-8}.$$

This type of a fine grid mesh for the y and z directions was chosen in order to properly resolve the velocity and viscous shear layers, and to more accurately define the conjugate heat transfer at the surface of the channel, thereby improving the temperature resolution. Furthermore, comparison with standard theoretical or numerical results, indicates that the finer the mesh size, the

higher the numerical accuracy. Detailed information about the validation of the numerical code and the systematic errors induced are presented in the next section. The reasons for the comparative coarse discretization for the x-direction are: (i) with the exception of the inlet region, the temperature gradients are small compared to the gradients occurring in other directions; and (ii) The CPU time as well as the memory storage required increases dramatically as the number of grid nodes is increased.

3. Validation of the code

Velocity field: The velocity field can be determined analytically using a more direct, although somewhat less accurate approach than the Fourier series approach for Eq. (6). As indicated by Bejan [14], the following approximation yields reasonably approximate results for this type of problem,

$$u(y,z) = \frac{9}{4}u_{\mathrm{m}}\left[1-\left(\frac{y}{H/2}\right)^2\right]\left[1-\left(\frac{z}{W/2}\right)^2\right] \tag{12}$$

and

$$\Delta P = f\frac{4L_x}{D_{\mathrm{h}}}\left(\frac{1}{2}\rho u_{\mathrm{m}}^2\right) \tag{13}$$

$$f = \frac{H^2+W^2}{(H+W)^2}\frac{24}{Re_{D_{\mathrm{h}}}} \tag{14}$$

$$Re_{D_{\mathrm{h}}} = \frac{u_{\mathrm{m}}D_{\mathrm{h}}}{\upsilon} \tag{15}$$

$$D_{\mathrm{h}} = \frac{4A}{\Gamma} = \frac{4HW}{2(H+W)} \tag{16}$$

Substituting Eqs. (14)–(16) into Eq. (13), the mean velocity for a given pressure drop, u_{m} can be obtained. Then, using the resulting value for u_{m} and Eq. (12), the approximate theoretical velocity distribution in the microchannel as shown in Fig. 3(a) can be obtained. Although a more accurate analytical solution was obtained by Shah and London [18], the method described above was chosen so that the numerical results can be evaluated and the various nondimensional parameters could be identified and used in the analysis and discussion of the results.

The numerically determined velocity field developed here is shown in Fig. 3(b). Comparison of the theoretical and numerical results indicates that while the numerical code accurately represents the general trend of the results, there is some disparity between the theoretical and numerical results, especially in the maximum value and the overall distribution around this maximum value. The small difference of the velocity profile between Fig. 3(a) and (b) is due to the approximations in the theoretical

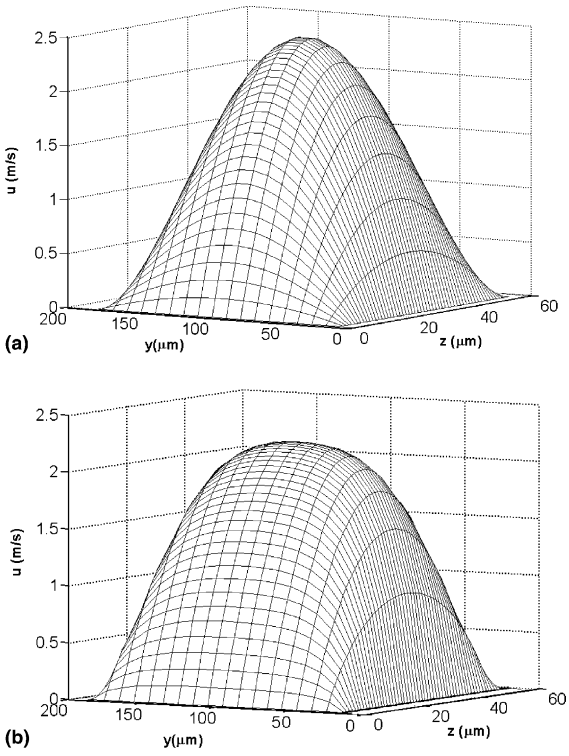

Fig. 3. Comparison of 2D velocity field between the approximate theoretical solution and the numerical result. (a) 2D velocity field in channel from the approximate theoretical expression Eq. (12) ($\Delta P = 50$ kPa, $Re = 99$, $T_{\mathrm{reference}} = 20$ °C, the mean velocity is 1.15 m/s). (b) 2D velocity field in channel from the numerical calculation ($\Delta P = 50$ kPa, $Re = 96$, $T_{\mathrm{reference}} = 20$ °C, the mean velocity is 1.11 m/s).

solution described in Eq. (12). But clearly, as evidenced by the magnitude of the mean velocities and the Reynolds numbers obtained from the different methods, the agreement between the two methods is quite good and provides sufficient evidence for validation of the method proposed here. In this comparison, the thermal properties of water were chosen at a temperature of 293 K (20 °C). Because the thermophysical properties are temperature dependent, particularly the liquid viscosity, the velocity and consequently the Reynolds numbers are different under the same pressure drop conditions. This issue will be discussed in more detail later. Fig. 4 compares the theoretical friction coefficient as determined from Eq. (14) with the numerical results obtained using the following procedure. The mass flow rate is calculated from the velocity as,

$$\dot{m} = \sum\sum \rho_{\mathrm{l}} \cdot u(j,k)\Delta y \Delta z \tag{17}$$

and then, the mean velocity is obtained as

$$u_{\mathrm{m}} = \frac{\dot{m}}{\rho_{\mathrm{l}} A} \tag{18}$$

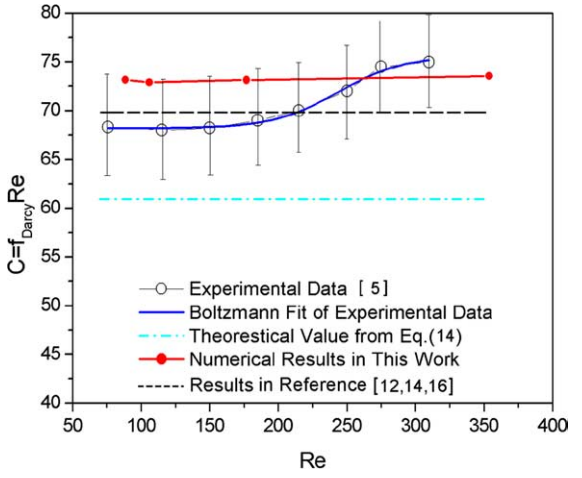

Fig. 4. Comparison among the numerical calculations, the theoretical predictions and the experimental data for the friction coefficient.

then using Eq. (13), the friction factor can be determined. In Refs. [14,16], the friction coefficient, $f\,Re$, is determined numerically for different duct cross-sections. For the rectangular channel with an aspect ratio (height to width) of 3–1 ($H:W$), which approximates the geometry used here, 180 μm × 57 μm, the Darcy friction factor–Reynolds number product, $f_{\mathrm{Darcy}}\,Re_{D_{\mathrm{h}}}$, is 69. The agreement between the numerical calculations here and the calculations obtained by others [14,16] indicates that the numerical code developed here is quite accurate for the fully developed laminar flow. Eq. (14) underestimates the friction factor since Eq. (14) was derived from an expected approximate velocity field Eq. (12).

In order to validate the assumption of fully developed flow in the microchannel, a 3D numerical simulation was performed using a commercial software package [FLUENT] to solve Eqs. (2), (3) and (5). The results are shown in Fig. 5, where the shadowed area represents the entrance region. The function of this 3D simulation for the fluid flow in microchannels is to:

(i) Identify the entrance length—the 3D simulation of fluid flow in the microchannel indicates that the length of the entrance region is in a range predicted by Eq. (1).
(ii) Validate the code developed here with one that is commercially available—the commercial code results and the results from the code developed in this work are in good agreement and as shown in Fig. 5, the 3D simulation of the velocity profile closely approximates the results shown in Fig. 3b.
(iii) Determine if for low mass flow rates (or low Reynolds numbers), the fully developed laminar flow assumption is correct—the experimental results of Kawano et al. [3] shown in Fig. 4, for a microchannel heat sink with the same channel geometry investigated here, indicate that if the Reynolds number is less than 200, the friction coefficient C is approximately 68 and constant. However, if the Reynolds number increases to a value above 200, the friction coefficient C increases with increases in the Reynolds number.

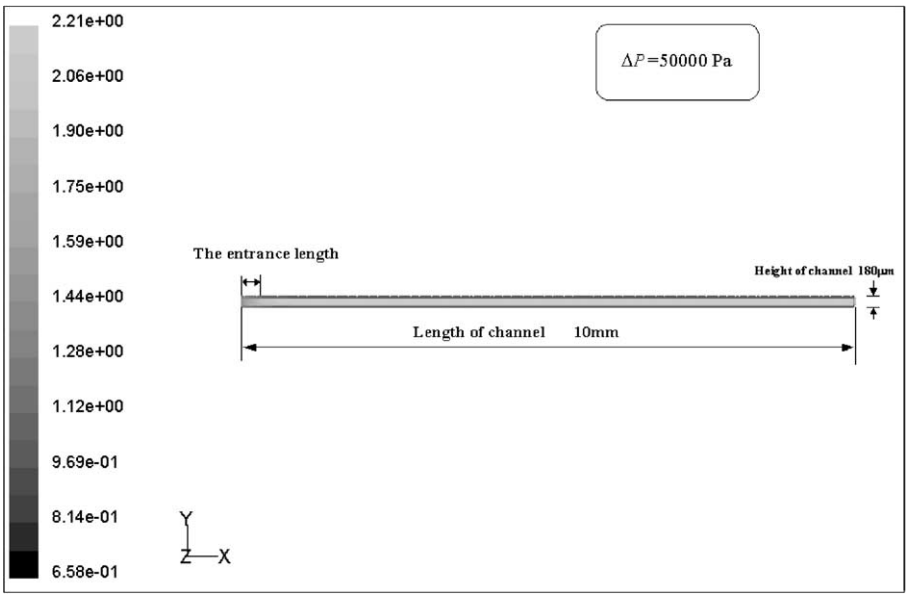

Fig. 5. 3D velocity field in the cross-section $z = L_z/2$ (refer to Fig. 2) of the channel from commercial code ($\Delta P = 50$ kPa, $T_{\mathrm{reference}} = 20$ °C).

Heat transfer: The code was first validated for one-dimensional heat conduction by comparing the results with a 1D analytical solution of heat conduction with a specified boundary condition [14]. The agreement was quite good and indicated very good correlation between the numerical results and the 1D analytical solution. Secondly, using conservation of energy, it can be shown that the maximum possible temperature rise between the fluid inlet and outlet i.e., no heat loss to the environment, can be expressed as:

$$\Delta T_{\mathrm{l,con}} = \frac{q_{\mathrm{w}} \cdot A_{\mathrm{w}}}{\dot{m}_{\mathrm{num}} \cdot C_P} \tag{19}$$

In addition, the average temperature rise between the inlet and outlet of the channel can be determined from the enthalpy increase as determined from the energy balance and can be expressed as:

$$\begin{aligned}\Delta T_{\mathrm{l,ave}} &= \overline{T}_{\mathrm{l}}(x = L_x) - \overline{T}_{\mathrm{l}}(x = 0) \\ &= \frac{\{\sum\sum \rho_{\mathrm{l}} \cdot u(j,k) \cdot C_P \cdot T(i = 20, j, k)\Delta y \Delta z - \sum\sum \rho_{\mathrm{l}} \cdot u(j,k) \cdot C_P \cdot T(i = 1, j, k)\Delta y \Delta z\}}{\dot{m}_{\mathrm{num}} \cdot C_P}\end{aligned} \tag{20}$$

In the current investigation, three different cases ($q_{\mathrm{w}} = 90$ W/cm^2, $\Delta P = 50$, 15, and 6 kPa) were explored.

Comparison of the results, indicates that the difference between $\Delta T_{\mathrm{l,ave}}$ (≈11.5, 36.7, 85.2 °C as determined by Eq. (20) for $q_{\mathrm{w}} = 90$ W/cm^2, $Re = 144$, 77, 42, respectively,) and $\Delta T_{\mathrm{l,con}}$ (≈14.3, 38.9, 86.5 °C as determined by Eq. (19), respectively, for the same conditions) is small. Differences of this magnitude can be attributed to (i) Eq. (19)—the maximum possible temperature rise in the bulk liquid from the energy balance; (ii) the mesh size is not as fine as required (infinitesimal), hence the accuracy of the statistical result from Eq. (20) is limited; or (iii) as mentioned above, the mesh size in the x-direction is comparatively coarse. A grid sensitivity analysis indicated that the accuracy of the velocity and temperature fields were heavily dependent on the grid size within the numerical domain. This is a truncation error involved in the numerical method. From the above comparison and discussion, the model developed here is consistent with the energy conservation law.

Further validation of the numerical results can be performed by comparison with the results provided in Refs. [10,12]. While some of these results are in good agreement, from a detailed analysis it is apparent that several new observations can be made which further clarify the results previously published in Refs. [10,12].

4. Results and discussion

A series of numerical calculations have been conducted and the results are presented in order to show the effects of heat flux and mass flow rate on the temperature distribution in the microchannel heat sinks. The following three subsections are devoted to the local temperature distribution in micro-heat sinks, the average bulk characteristics of heat transfer, and further general discussion. Furthermore, in order to better compare the computational results obtained here with the experimental data available in the literature, the average overall Nusselt number is defined and analyzed with respect to the variations in the Reynolds number.

4.1. Local temperature distributions

Fig. 6 shows a velocity field in a microchannel (with the vertical scale different from the horizontal scale) at $\Delta P = 50$ kPa. As discussed previously, the thermophysical properties of the liquid are based upon the estimated liquid bulk temperature. As can be seen by comparison with the results shown in Fig. 3, for the same pressure drop along the channel, the thermal properties, velocity profile, mean velocity and Reynolds number are all significantly different. This difference demonstrates how significant the variation of the thermophysical properties of the liquid with respect to temperature can be. As shown, a variation in the reference temperature $T_{\mathrm{reference}}$ from 20 to 32 °C, changes the mean velocity from 1.11 to 1.31 m/s, and results in a corresponding change in the Reynolds number from 96 to 144.

The numerical results for the temperature distribution in the heat sinks are shown in Figs. 7 and 8 for different locations along the channel. Fig. 7a–c show the local cross-sectional temperature distribution in the y–z plane at $x = 0$, $x = L_x/2$ and $x = L_x$, respectively. As shown in Fig. 7a, the temperature of the liquid at the inlet is initially uniform (at 20 °C). The temperature profiles shown in Fig. 7b and c are similar in shape due to the assumption of hydrodynamic fully developed flow, but the magnitudes of the temperature are different. Fig. 8a illustrates the temperature contours in the heat sink at the outlet of the channel and Fig. 8b shows the local temperatures inside the channel. It is interesting to note in Fig. 8b that the temperature is highest at the channel corner. This is due to the low velocity of the flow and the resulting high concentration of heat flux, causing bubble nucleation in the channel corner [19]. In a majority of the published literature, it is assumed that the measured substrate wall temperature is the boiling incipience point for the liquid. From these calculations it

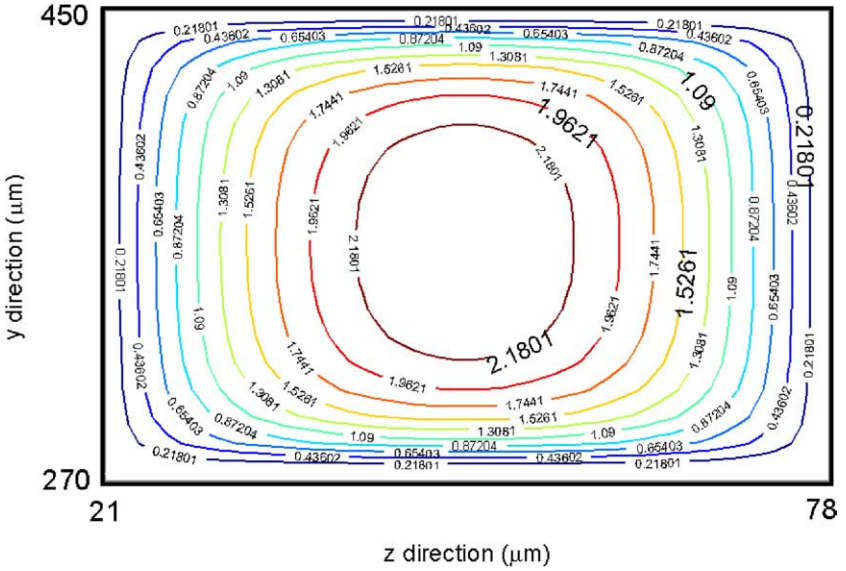

Fig. 6. 2D velocity field in channel from the numerical calculation ($\Delta P = 50$ kPa, $Re \approx 144$, $T_{\text{reference}} = 32$ °C, the mean velocity is 1.312 m/s).

is apparent that there is a 2–3 °C temperature difference between the bottom wall of the substrate and the bottom surface of the channel.

The temperature distribution can be illustrated more clearly in Fig. 9a–c, which represent the local temperature distribution in the x–y plane at $z = L_z/2$ for the three cases with $q_w = 90$ W/cm^2, at $\Delta P = 50$, 15 and 6 kPa, respectively. The temperature variations in the bulk liquid and the substrate are represented by variations in the color, with the temperature scale located at the side of each figure. The liquid flow is clearly apparent in this figure, which when combined with Figs. 7 and 9 yield detailed information about the temperature distribution in the micro-heat sink.

4.2. Average and bulk heat transfer characteristics

As discussed previously, Fedorov and Viskanta [12] presented a detailed distribution of the local heat flux at the inner wall of the channel where the solid and the fluid are in direct contact. Similarly, Qu and Mudawar [10] also analyzed the local heat flux and the local Nusselt number distribution at the inner channel wall. Both of those analyses depended on the different definitions of the local heat flux and the local Nusselt number.

In order to evaluate the local averaged heat transfer characteristics along the flow direction, the convective heat transfer coefficient and Nusselt number, must be defined. For purposes of the current investigation, the longitudinal convective heat transfer coefficient is defined as

$$\bar{h}_x = \frac{\bar{q}_{s,\Gamma}(x)}{\Delta \overline{T}(x)} \tag{21}$$

and the averaged longitudinal Nusselt number as

$$\overline{Nu}_x = \frac{\bar{h}_x \cdot D_h}{\lambda_l} \tag{22}$$

The averaged longitudinal local heat flux along the perimeter of the inner wall of the channel in Eq. (21) is defined and calculated as

$$\begin{aligned} \bar{q}_{s,\Gamma}(x) &= -\lambda_w \left(\frac{\partial T_w(x,y,z)}{\partial n}\bigg|_\Gamma \right) \\ &= -\lambda_l \left(\frac{\partial T_l(x,y,z)}{\partial n}\bigg|_\Gamma \right) \end{aligned} \tag{23}$$

and the longitudinal mean temperature difference in Eq. (21) is defined as,

$$\Delta \overline{T}(x) = \overline{T}_{w,\Gamma}(x) - \overline{T}_l(x) \tag{24}$$

here,

$$\overline{T}_{w,\Gamma}(x) = \frac{\sum_\Gamma T_{w,\Gamma}(i,j,k)}{N_\Gamma},$$

$$\overline{T}_l(x) = \frac{\sum\sum \rho_l \cdot u(j,k) \cdot C_P \cdot T_l(i,j,k) \Delta y \Delta z}{\dot{m}_{\text{num}} \cdot C_P},$$

where N_Γ is the total number of nodes along the perimeter of the inner wall (here $N_\Gamma = 2 \times 18 + 2 \times 57$). The averaged longitudinal inner wall temperature $\overline{T}_{w,\Gamma}(x)$ and the averaged local heat flux $\bar{q}_{s,\Gamma}(x)$ are mathematically averaged along the perimeter of the

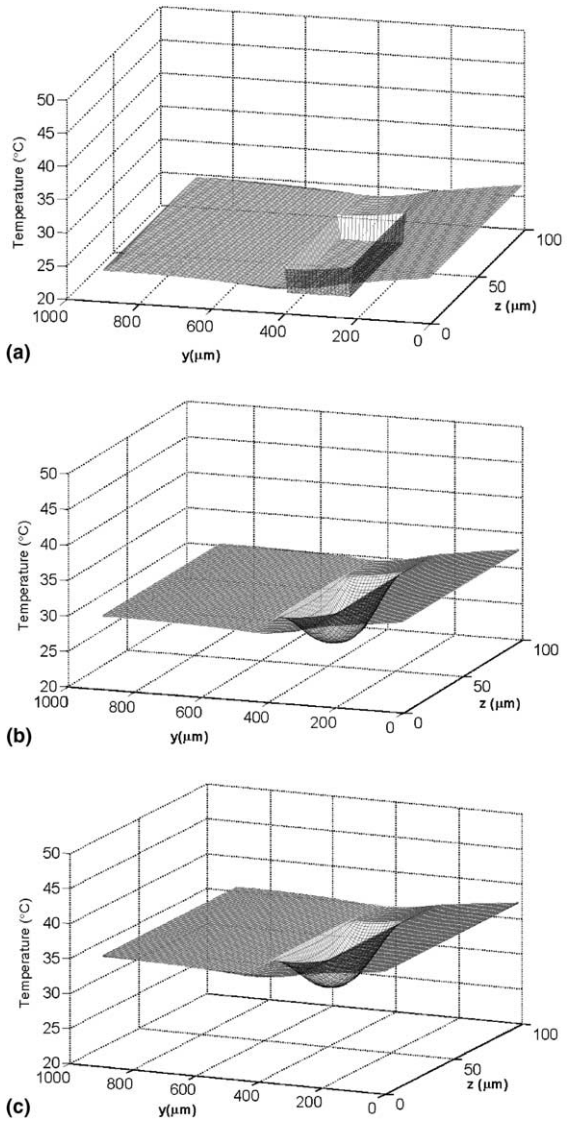

Fig. 7. Local temperature distribution in y–z plane at different x location along the flow direction ($\Delta P = 50$ kPa, $Re \approx 144$, $T_{\text{reference}} = 32$ °C, the mean velocity is 1.312 m/s). (a) $x = 0$, (b) $x = L_x/2$ (5 mm), (c) $x = L_x$ (10 mm).

inner wall, and the longitudinal bulk liquid temperature $\overline{T}_l(x)$ is averaged according to energy conservation.

With Eqs. (22)–(24), the longitudinal heat transfer coefficient variation and the longitudinal Nusselt number variation for these three cases can be determined and are shown in Figs. 10 and 11, respectively. The thermal entrance lengths for these three cases are 4, 2, and 1 mm, respectively. From these two figures it can be concluded that the variations of the heat transfer coefficient and the Nusselt number along the flow direction is quite small for this type of microchannel heat sink after the thermal entrance lengths (the simplest type). It should be noted that since the grid size in the flow direction is relatively coarse, the local heat transfer is not as accurate or detailed as is the case for the y- and z-direction. However, the resolution is sufficient to aid in the design of microheat sinks for industrial applications and also to provide information and insight into the fluid flow characteristics in the flow direction.

4.3. Further discussion

The principal issues in heat sink design are the overall heat transfer performance (for electronic cooling) and the local temperature gradient (for determining the thermal stress). While a number of investigations are currently underway to actually measure the temperature and pressure gradients in these microchannels, no experimental data are currently available.

In order to aid in the prediction of the thermal and fluid flow characteristics, a correlation is developed here based upon the numerical results shown in Fig. 11. Using the proportionally averaged equivalent value $\overline{Nu}_{\text{eq}}$ of the local $\overline{Nu}_x$ number in the longitudinal direction as shown in Fig. 11, the conventional form of the correlation for the Nusselt number as given in [16] and fitting the data obtained, the following correlation can be developed for the overall equivalent Nusselt number (the datas of $\overline{Nu}_{\text{eq}}$ are shown in Table 2 (the sixth column). Another three more cases are calculated to ensure the correctness of the correlation developed in this article (the results are also shown in Table 2),

$$\overline{Nu}_{\text{eq}} = 4.1 + \frac{0.14 \cdot (D_h/L) \cdot Re_D \cdot Pr}{1 + 0.05[(D_h/L) \cdot Re_D \cdot Pr]^{2/3}} \tag{25}$$

Here, the reference temperature for the thermophysical properties of water was chosen as $T_{\text{reference}} = (T_{l,\text{in}} + T_{l,\text{out}})/2$. The corresponding thermal and hydrodynamic parameters are given in Table 2. For the cases investigated here, the Prandtl number, Pr, is not an independent parameter, since Pr is chosen based upon the reference temperature $T_{\text{reference}}$ and this value, $T_{\text{reference}}$, is calculated from the energy balance for each pressure drop (or Re number) using Eq. (19). It is apparent here that the asymptote, $\overline{Nu} = 4.1$, lies between the values for a constant axial wall heat flux, 4.8, and a constant axial wall temperature, 4.0, for fully developed laminar flow in ducts, of rectangular cross-section with ($W : H = 1 : 3$). It should be noted here that Eq. (25) is specifically for the water/silicon system and for the specific geometry of the heat sink used in this work. Comparisons between the predicted results given by Eq. (25) and the numerical results are plotted in Figs. 12 and 13. If the error is estimated to be 5% or less, it is apparent that Eq. (25) can be used to accurately predict the Nusselt number. It should also be noted that based

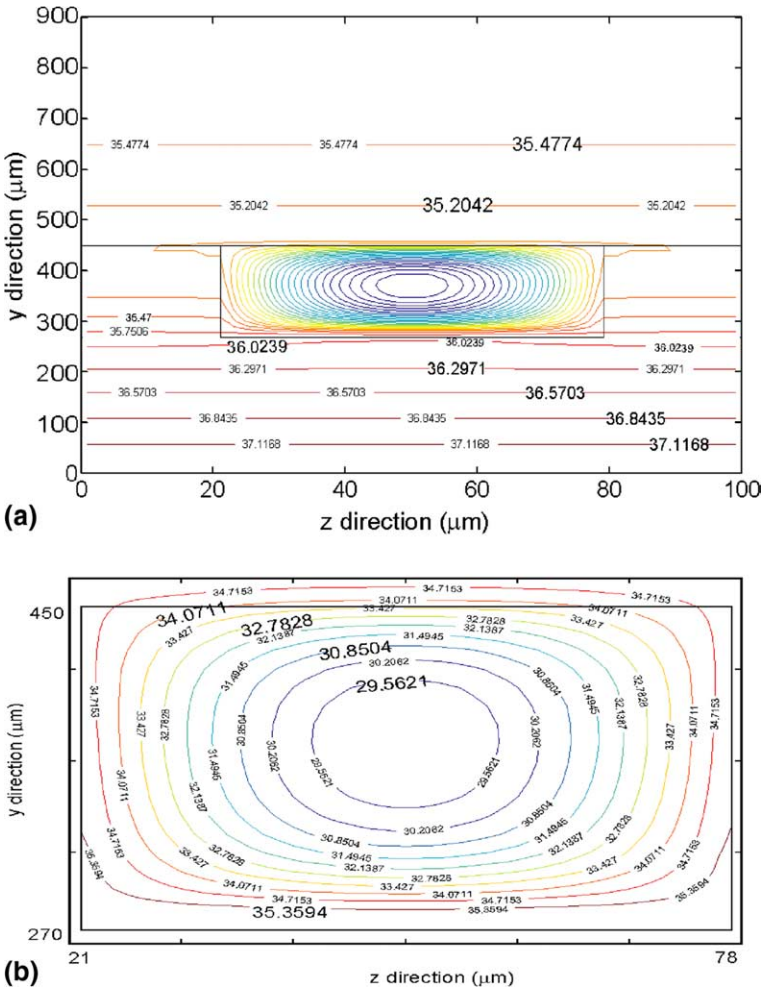

Fig. 8. Contour of temperature in the heat sink at the cross-section of the outlet of the channel ($\Delta P = 50$ kPa, $Re \approx 144$, $T_{\text{reference}} = 32$ °C, the mean velocity is 1.312 m/s). (a) Temperature in the heat sink, (b) local temperature inside the channel.

upon Fig. 11 the asymptote for the average longitudinal Nusselt number, $\overline{Nu}_x$, should be approximately 4.0. Because of the limitations in the grid size used in the numerical simulation developed here and with the obtained equivalent $\overline{Nu}_{\text{eq}}$ as shown in Table 2, a value of 4.1 is proposed for the thermal fully developed flow under such conditions.

In many previous investigations, the average heat transfer coefficient is simply defined as $\bar{h} = \frac{q_w}{\Delta \overline{T}_{\text{ave}}}$ which is determined based upon the heat flux density applied to the bottom of the substrate and the temperature difference between the average substrate wall temperature and the bulk liquid temperature $(\Delta \overline{T}_{\text{ave}} = \overline{T}_w(x) - \overline{T}_l(x))$. However, this definition does not consider the true convective heat transfer surface, which is the total surface area of the inner wall of the channel instead of the bottom surface of the substrate. Thus, the expression $\bar{h} = \frac{q_w}{\Delta \overline{T}_{\text{ave}}}$, significantly overestimates the heat transfer coefficient by a factor equal to the relative area ratio between the total inner wall surface area and the surface area of the bottom of the substrate. From an energy balance, a more accurate estimation of the convective heat transfer coefficient can be expressed as,

$$q_w \cdot A_w = \bar{h}_x \cdot S \cdot (\overline{T}_w(x) - \overline{T}_l(x)) \tag{26}$$

where, $A_w = L_x \cdot L_z$, $S = L_x \cdot (2W + 2H)$, and $\overline{T}_w(x) = \frac{\sum_{k=1}^{99} T_w(i,j=1,k)}{99}$, and the local Nusselt number is

$$\overline{Nu}_x = \frac{\bar{h}_x \cdot D_h}{\lambda_l} \tag{27}$$

Fig. 14 illustrates the longitudinal mean temperature variations at the bottom wall and in the bulk liquid for

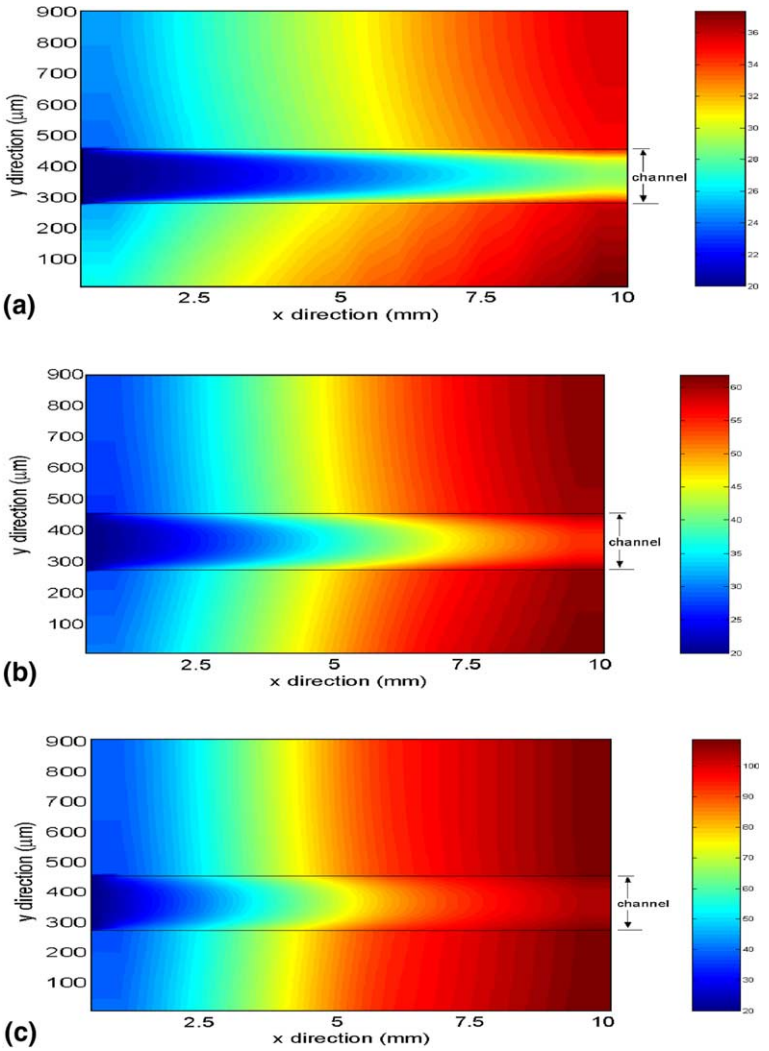

Fig. 9. Local temperature distribution in x–y plane at $z = L_z/2$. (a) $\Delta P = 50$ kPa, $Re \approx 144$, $T_{\text{reference}} = 32$ °C, the mean velocity is 1.312 m/s; (b) $\Delta P = 15$ kPa, $Re \approx 77$, $T_{\text{reference}} = 47$ °C, the mean velocity is 0.526 m/s; (c) $\Delta P = 6$ kPa, $Re \approx 42$, $T_{\text{reference}} = 57$ °C, the mean velocity is 0.249 m/s. The temperature at the outlet for the case of $\Delta P = 6$ kPa is higher than 100 °C where boiling may occur. Therefore, the numerical solution for single-phase flow may not be valid there.

the three cases evaluated here. As shown, the bulk temperature variation in the liquid along the flow direction assumes a quasi-linear form for high mass flow rates or large Reynolds numbers.

The results of the local Nusselt number $\overline{Nu}_{x,\text{rough}}$ calculated from Eqs. (26) and (27) are plotted in Fig. 15. If the data, shown in Fig. 15 are compared with the detailed results shown in Fig. 11, it is apparent that if the definitions for the heat transfer coefficient and Nusselt number, Eqs. (26) and (27), respectively, are used, the heat transfer will be underestimated at the entrance portion of the channel (especially close to the inlet) and overestimated towards the end of the channel. Eqs. (26) and (27) do not consider either the heat conduction in the substrate and the conjugate heat transfer influence on the local heat flux variation along the longitudinal direction, or the flow direction. From the temperature distribution in the heat sink shown in Fig. 9a–c, the temperature gradient in the substrate and liquid are calculated for the different cases and are shown in Fig. 16a–c, respectively. If the heat flux distribution is evaluated from the temperature gradient with $\vec{q} = -\lambda \nabla T$, it is apparent that the heat in the substrate will be conducted into the front part of the heat sink due to the temperature gradient, especially for low liquid flow rates. From Fig. 16a, it is apparent that only a small portion of the heat is conducted into the front part of the heat sink due to the high liquid velocity. From Fig.

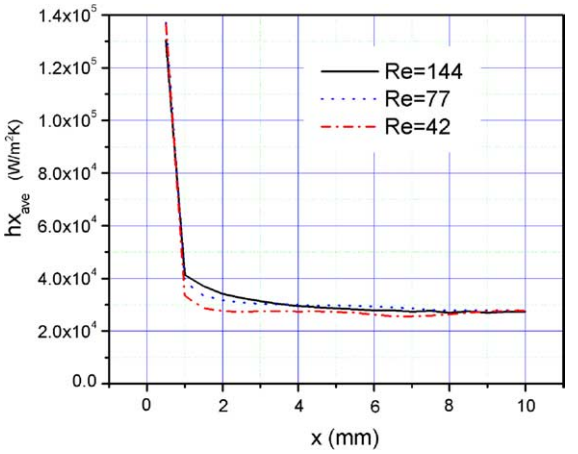

Fig. 10. Longitudinal heat transfer coefficient variation for the three different cases ($\Delta P = 50$, 15 and 6 kPa).

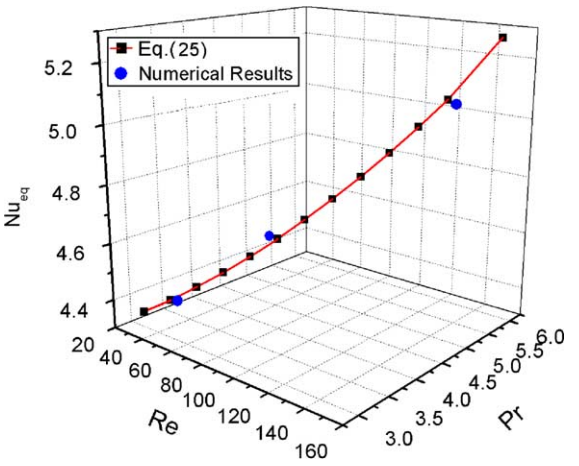

Fig. 12. The predicted values from the correlation Eq. (25) developed in this work and the numerical results for overall equivalent *Nu* number.

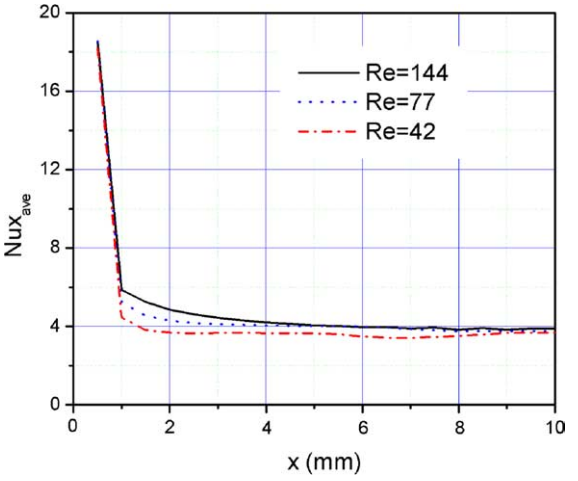

Fig. 11. Longitudinal Nusselt number variation for the three cases ($\Delta P = 50$, 15 and 6 kPa).

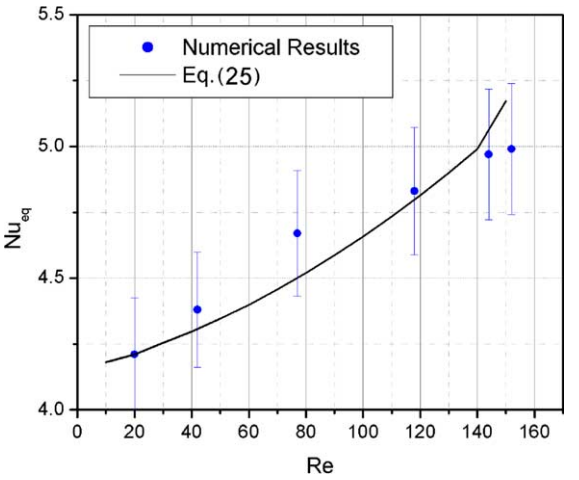

Fig. 13. Comparison between the predicted values from Eq. (25) and the numerical results for overall equivalent *Nu* number.

Table 2
Thermal and hydrodynamic parameters and overall *Nu* number from calculations[a]

Cases	ΔP (kPa)	$T_{reference}$ (°C)	*Re*	*Pr*	$\overline{Nu}_{eq}$	$\overline{Nu}_{rough}$	$\overline{Nu}_{definition}$
1	50	32	144	5.25	4.97	4.08	4.23
2	15	47	77	3.8	4.67	3.45	3.57
3	6	57	42	3.2	4.38	3.69	3.16
4	65	27	152	5.9	4.99	4.26	4.34
5	35	37	118	4.6	4.83	3.65	3.91
6[b]	3	57	20	3.2	4.21	5.61	2.28

[a] The thermal properties of water are adopted from Ref. [16].
[b] The heat flux is 40 W/cm^2.

16c a large portion of heat is conducted into the front part of the heat sink due to the low liquid velocity. This is the reason why the temperature variations in Fig. 14 have different gradients, especially at the front part of

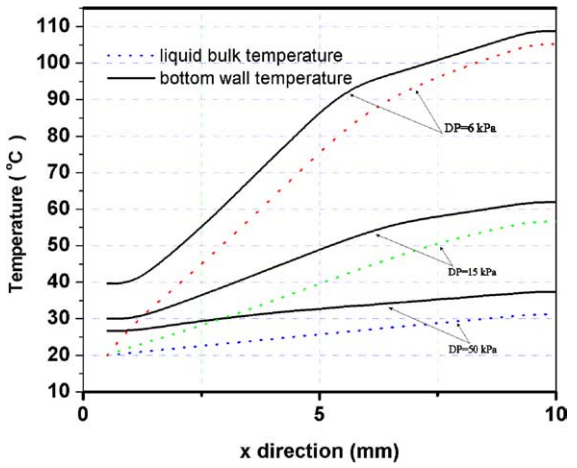

Fig. 14. Longitudinal mean temperature variations at the bottom wall and in bulk liquid.

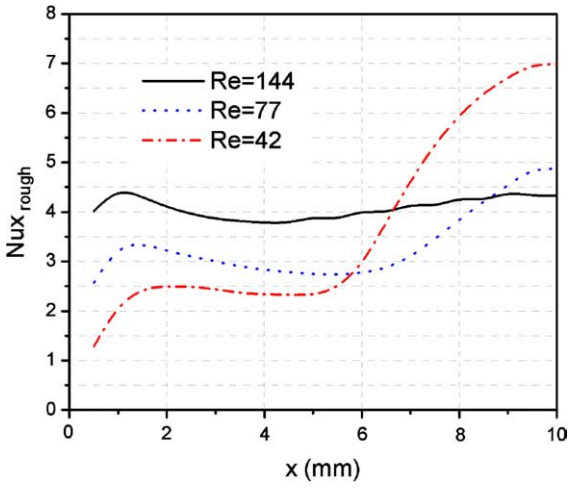

Fig. 15. The results of the local Nusselt number calculated from a rough definition of the heat transfer coefficient.

the curves. For these reasons, the Nusselt number can be approximated from Eqs. (26) and (27) and is shown as $\overline{Nu}_{x,\text{rough}}$. An enlarged view of temperature gradient in the substrate and at the inside wall close to the entrance is shown in Fig. 17. Here the thermal entrance is clearly apparent, e.g., as shown in Fig. 17(a) after 2.5 mm the heat flux at the inside wall of channel still varies for $Re = 144$, but as shown in Fig. 17(b) after 1 mm the heat flux does not change at the inside wall of channel for $Re = 42$, which agrees with the results as shown in Fig. 11.

The roughly averaged overall Nusselt number from, $\overline{Nu}_{\text{rough}}$, can be obtained for the different cases, which is proportionally mathematically averaged on the basis of $\overline{Nu}_{x,\text{rough}}$ shown in Fig. 15. The results are shown in Table 2 (the seventh column), which indicates that even though the magnitude of the average Nusselt number $\overline{Nu}_{\text{rough}}$ obtained from Eq. (27), i.e., using an energy balance, agrees reasonably well with the average Nusselt number $\overline{Nu}_{\text{eq}}$ from the detailed and more accurate analysis given in Eq. (21)–(24), the trend of the $\overline{Nu}_{\text{rough}}$ with respect to the variation of the Reynolds number is incorrect for the reasons outlined above. This raises another issue and that is how to interpret the experimental results for these types of investigations. The following considerations must be taken into account in the evaluation of any experimental results:

(1) Because to date all of the experimental data utilizes the temperature at the substrate wall and at the inlet and outlet of the channel, simply using the data reduction described in Eqs. (26) and (27) may lead to an incorrect conclusion as may have been the case in [20]. A general review of this topic can be found in Ref. [21].
(2) Since it is difficult to measure the local heat flux at the inner wall of the channel, the definition of the heat transfer coefficient is very important and will strongly influence the results and how the heat transfer varies in micro-heat sinks.

In order to determine an optimal definition for the heat transfer coefficient and Nusselt number for use in evaluating experimental results, a comparison of the different definitions was conducted to evaluate the merits of the various definitions that either might or have been used previously. If the following definition is utilized, the results approach the numerically predicted values and also represent the correct variation of the Nusselt number with respect to the Reynolds number,

$$\Delta T(x) = \frac{(\Delta\overline{T}(x) - \Delta\overline{T}_{\text{ave}})}{\ln(\Delta\overline{T}(x)/\Delta\overline{T}_{\text{ave}})} \tag{28}$$

where $\Delta\overline{T}(x) = \overline{T}_{\text{w}}(x) - \overline{T}_{\text{l}}(x)$, $\Delta\overline{T}_{\text{ave}} = \overline{T}_{w,\text{ave}} - \overline{T}_{\text{l,ave}}$ and $\overline{T}_{w,\text{ave}}$, $\overline{T}_{\text{l,ave}}$ are mathematically averaged values from $\overline{T}_{\text{w}}(x)$, $\overline{T}_{\text{l}}(x)$, respectively. For experimental data processing, $\overline{T}_{w,\text{ave}}$, $\overline{T}_{\text{l,ave}}$ are the averaged values from the measured temperature of the liquid and substrate wall respectively along the flow direction. From a heat transfer perspective, a log-mean temperature difference (LMTD) has been used to describe the temperature variation in the longitudinal direction. This parameter allows the overall averaged temperature difference, $\Delta\overline{T}_{\text{ave}}$, to be used as a comparative value to compensate for the different heat flux densities in the longitudinal direction. If the definition of $\Delta T(x)$ of Eq. (28) is substituted into Eq. (26) replacing $\Delta\overline{T}_{\text{ave}}$, an overall, but more reasonable average Nusselt number $\overline{Nu}_{\text{definition}}$ is obtained, based on the numerical results as shown in Fig. 11. The resulting parameter $\overline{Nu}_{\text{definition}}$ is shown in

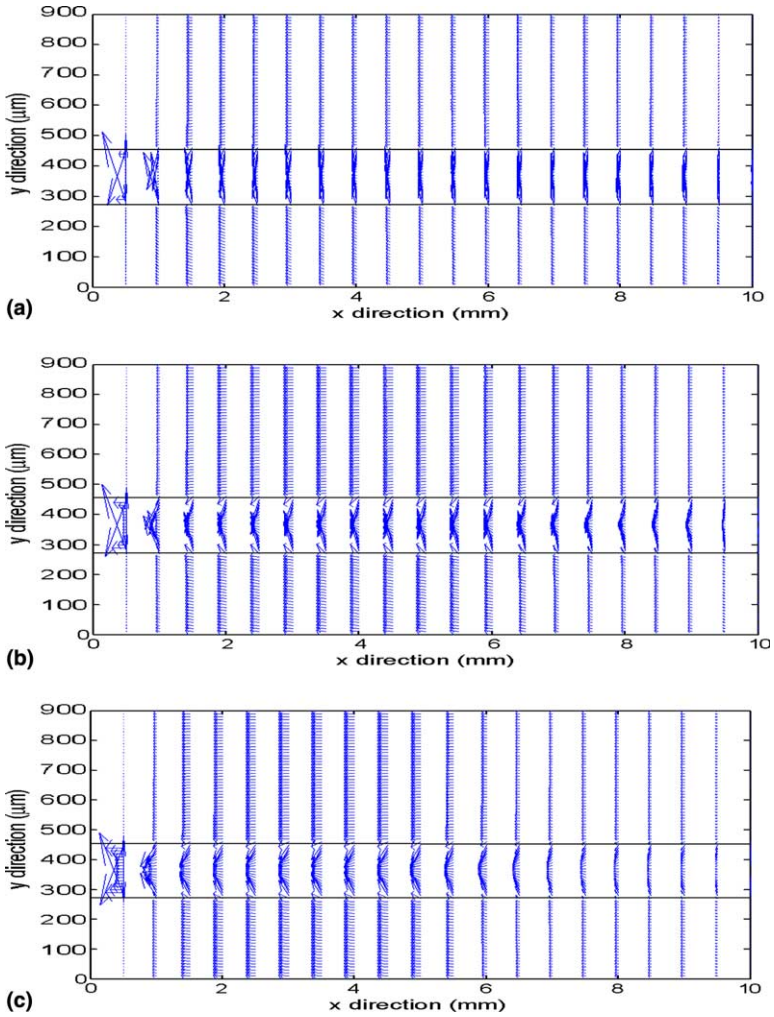

Fig. 16. Heat flux distribution in substrate and liquid. (a) $\Delta P = 50$ kPa, $Re \approx 144$, $T_{\text{reference}} = 32$ °C, the mean velocity is 1.312 m/s; (b) $\Delta P = 15$ kPa, $Re \approx 77$, $T_{\text{reference}} = 47$ °C, the mean velocity is 0.526 m/s; (c) $\Delta P = 6$ kPa, $Re \approx 42$, $T_{\text{reference}} = 57$ °C, the mean velocity is 0.249 m/s.

the last column of Table 2. As shown, the difference in the Nusselt number between the accurate analysis of the local heat transfer $\overline{Nu}_{\text{eq}}$ and the result from the definition Eq. (28) $\overline{Nu}_{\text{definition}}$ is approximately 1. The principal reason for this difference is that the local heat flux density at the inner wall of the channel is typically not measured and can only be estimated from the substrate wall temperature and the liquid bulk temperature.

Based upon the analysis performed here, it is clear that the definition given in Eq. (28), can be used with Eqs. (26) and (27) to correctly interpret the limited data (the substrate wall temperature and the inlet and outlet liquid bulk temperature) obtained experimentally.

Another important issue related to the experiment is the heat loss associated with the longitudinal heat conduction from the substrate to the ambient. From Fig. 16a–c it is apparent that the longitudinal heat conduction along the silicon wafer at different Reynolds numbers is different. The components of the heat flux vectors can be evaluated from the calculated temperature gradient as shown in Fig. 16a–c. As shown, for $Re = 140$, approximately 10% of the heat is conducted into the front part of the heat sink near the edge and approximately 20% of the heat is conducted into the front part of the heat sink in the middle region of the heat sink. However, for $Re = 40$, these values are approximately 40% and 60%, respectively. In reality, because it is difficult to achieve an adiabatic boundary at the inlet and outlet of the heat sink as assumed in the numerical model, a significant portion of the heat loss is transferred to the ambient environment, especially for low fluid flow conditions. Thus, when evaluating the heat

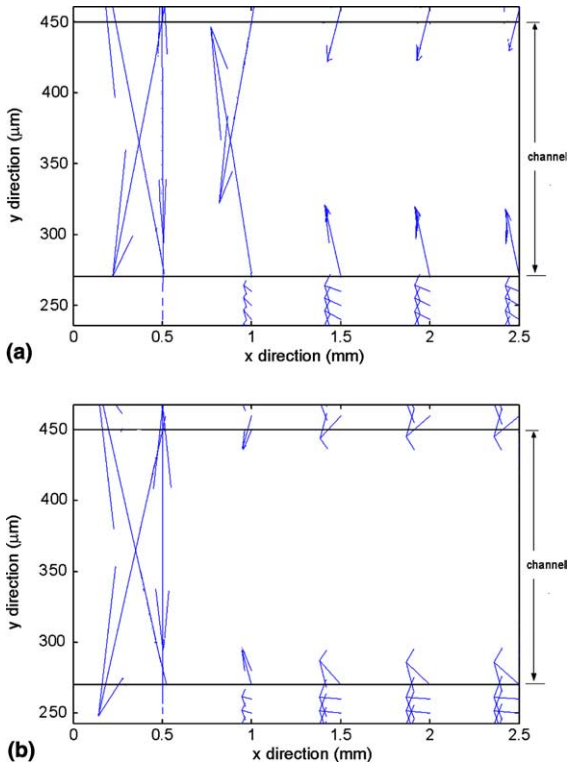

Fig. 17. Heat flux distribution in substrate close to the inlet. (a) $\Delta P = 50$ kPa, $Re \approx 144$, $T_{\text{reference}} = 32$ °C, the mean velocity is 1.312 m/s; (b) $\Delta P = 6$ kPa, $Re \approx 42$, $T_{\text{reference}} = 57$ °C, the mean velocity is 0.249 m/s.

transfer in micro-heat sinks with low fluid flow rates, particular attention should be paid to the effects of this heat loss.

5. Conclusions

A detailed numerical simulation of the heat transfer occurring in silicon-based microchannel heat sinks has been conducted using a simplified three-dimensional conjugate heat transfer model (2D fluid flow and 3D heat transfer). The micro-heat sink modeled consists of a 10 mm long silicon substrate, with rectangular microchannels, 57 μm wide and 180 μm deep, fabricated along the entire length. A finite difference numerical code was developed using a Tri-Diagonal Matrix Algorithm (TDMA) to solve the governing equations. The validated code provided detailed temperature and heat flux distributions in the microchannel heat sink. The influence of the geometric parameters of the channel and the thermophysical properties of the fluid on the flow and the heat transfer, are investigated using a temperature-dependent thermophysical property method. The results indicate that the thermophysical properties of the liquid can significantly influence both the flow and heat transfer in the microchannel heat sink. The bulk liquid temperature is shown to vary in a quasi-linear form along the flow direction for high fluid flow rates, but not for low flow rates. Comparison of the numerical results with other published numerical results and experimental data available in the literature for Reynolds numbers less than 200 based on a hydraulic diameter of $D_h = 86$ μm and $D_h/L_x < 0.01$, indicates that the assumption of hydrodynamic, fully developed laminar flow is valid. The thermal entrance length is also obtained from the detailed local heat transfer coefficient calculation and a correlation for the overall averaged Nusselt number with the Reynolds number is developed and discussed. The results indicate that variations in the way the Nusselt number is defined may result in different conclusions even using the same experimental data. For proper analysis of the experimental results, a methodology is proposed whereby measured data can be evaluated and processed in order to provide consistent interpretation, a more complete understanding and better interpretation of these experimental data.

Acknowledgements

The authors would like to acknowledge the support of the Office of Naval Research Grant ONR N000140010454 and the National Science Foundation CTS-0312848. The authors would also like to thank Dr. C.B. Sobhan for helpful discussion during the course of this study.

References

[1] I. Mudawar, Assessment of high-heat-flux thermal management schemes, IEEE. Trans. Compon. Pack. Technol. 24 (2) (2001) 122–141.
[2] G.E. Kendall, P. Griffith, A.E. Bergles, J.H. Lienhard V, Small diameter effects on internal flow boiling, in: Proceedings of 2001 ASME International Mechanical Engineering Congress and Exposition, New York, 2001, pp. 1–17.
[3] P. Rao, R.L. Webb, Effects of flow mal-distribution in parallel micro-channels, in: Proceedings of 34th National Heat Transfer Conference, Pittsburgh, 2000, pp. 1–9.
[4] X.F. Peng, G.P. Peterson, Convective heat transfer and flow friction for water flow in microchannel structures, Int. J. Heat Mass Transfer 39 (12) (1996) 2599–2608.
[5] K. Kawano, K. Minakami, H. Iwasaki, M. Ishizuka, Development of micro channels heat exchanging, in: R.A. Nelson Jr., L.W. Swanson, M.V.A. Bianchi, C. Camci (Eds.), Application of Heat Transfer in Equipment, Systems, and Education, HTD-Vol. 361-3/PID-Vol. 3, ASME, New York, 1998, pp. 173–180.

[6] H.Y. Wu, P. Cheng, Friction factors in smooth trapezoidal silicon microchannels with different aspect ratios, Int. J. Heat Mass Transfer 46 (14) (2003) 2519–2525.
[7] H.Y. Wu, P. Cheng, An experimental study of convective heat transfer in silicon microchannels with different surface conditions, Int. J. Heat Mass Transfer 46 (14) (2003) 2547–2556.
[8] M. Choi, K. Cho, Effect of the aspect ratio of rectangular channels on the heat transfer and hydrodynamics of paraffin slurry flow, Int. J. Heat Mass Transfer 44 (1) (2001) 55–61.
[9] G. Tunc, Y. Bayazitoglu, Heat transfer in rectangular microchannels, Int. J. Heat Mass Transfer 45 (4) (2002) 765–773.
[10] W. Qu, I. Mudawar, Analysis of three-dimensional heat transfer in micro-channel heat sinks, Int. J. Heat Mass Transfer 45 (2002) 3973–3985.
[11] A. Weisberg, H.H. Bau, J.N. Zemel, Analysis of microchannels for integrated cooling, Int. J. Heat Mass Transfer 35 (1992) 2465–2474.
[12] A.G. Fedorov, R. Viskanta, Three-dimensional conjugate heat transfer in the microchannel heat sink for electronic packaging, Int. J. Heat Mass Transfer 43 (3) (2000) 399–415.
[13] J.D. Parker, J.H. Boggs, E.F. Blick, Introduction to Fluid Mechanics and Heat Transfer, Addison-Wesley Publishing Company, Reading, MA, 1974.
[14] A. Bejan, Convection Heat Transfer, first ed., John Wiley & Sons, New York, 1984.
[15] S. Kakac, Y. Yener, Convective Heat Transfer, second ed., CRC Press, Begell House, Boca Raton, 1995.
[16] A.F. Mills, Heat Transfer, second ed., Prentice Hall, Upper Saddle River, 1999.
[17] S.V. Patankar, Numerical Heat Transfer and Fluid Flow, Hemisphere, Washington, DC, 1980.
[18] R.K. Shah, A.L. London, Laminar Flow Forced Convection in Ducts: a Source Book for Compact Heat Exchanger Analytical Data, Academic Press, New York, 1978.
[19] J. Li, P. Cheng, Bubble cavitation in a microchannel, Int. J. Heat Mass Transfer 47 (2004) 2689–2698.
[20] B.X. Wang, X.F. Peng, Experimental investigation on liquid forced convection heat transfer through microchannels, Int. J. Heat Mass Transfer 37 (1) (1994) 73–82.
[21] S.V. Garimella, C.B. Sobhan, Transport in microchannels—a critical review, Ann. Rev. Heat Transfer 13 (2003) 1–50.